Multicomponent time-lapse seismic interpretation of Rulison Field, Colorado using spectral-decomposition attributes

NELSON ROJAS, Ecopetrol S. A. THOMAS L. DAVIS, Colorado School of Mines

The most common applications of spectral decomposition I in seismic interpretation have been to delineate and visualize stratigraphic features and as a direct hydrocarbon indicator. In this study, we applied spectral decomposition to time-lapse seismic interpretation. We used the multicomponent seismic data acquired by the Reservoir Characterization Project of Colorado School of Mines at Rulison Field in 2003, 2004, and 2006.

Rulison Field is located in northwest Colorado's Piceance Basin (see Davis and Benson in April TLE 2009 for map of region). The Mesaverde Formation is a heterogeneous tightsandstone gas reservoir that produces from a thick gross interval (2000-2200 ft) of thin interbedded sandstones, coals, and shales deposited in a fluvial system (Figure 1). The gas is mainly produced from sandstone intervals, which have low porosities (4–8%), very low permeabilities (20–80 μ D), and contain natural fractures. A detailed geological description can be found in Cumella and Ostby (2003).

Time-lapse hypothesis

Previous work in Rulison Field found that both P-waves and S-waves change with the differential pressure at a constant confining pressure. The most probable range for velocity increase due to pressure drawdown in wells is 5-10%. This reservoir produces gas with small amounts of water. Thus no fluid substitution occurs; we assume that the velocity is the main parameter that affects the seismic data and that the gas production is one of the main variables to compare when doing time-lapse seismic interpretation.

The 4D seismic data cover 2.15 mi² and were integrated with well-log data (Figure 2).

Seismic data preparation

Although the data sets were processed with the same parameters and workflows, systematic differences in the data due to external factors are unavoidable and must be removed through a process called cross-equalization. 4D seismic data cross-equalization works with paired traces at the same position in space but from volumes acquired at different times. With the P-wave and pure S-wave data, we cross-equalized the 2003 survey with 2004 and with 2006. The converted shear-wave data were cross-equalized using the seismic volumes of 2003 and 2006. With both pure and converted S-waves, we cross-equalized the fast- and slow-wave modes separately.

The objective of cross-equalization is to remove timing and wavelet differences in common trace pairs that occur where no differences are expected. The zone or interval where no change is expected is called the "static window." In the Rulison Field data, the interval of 700-925 ms was chosen

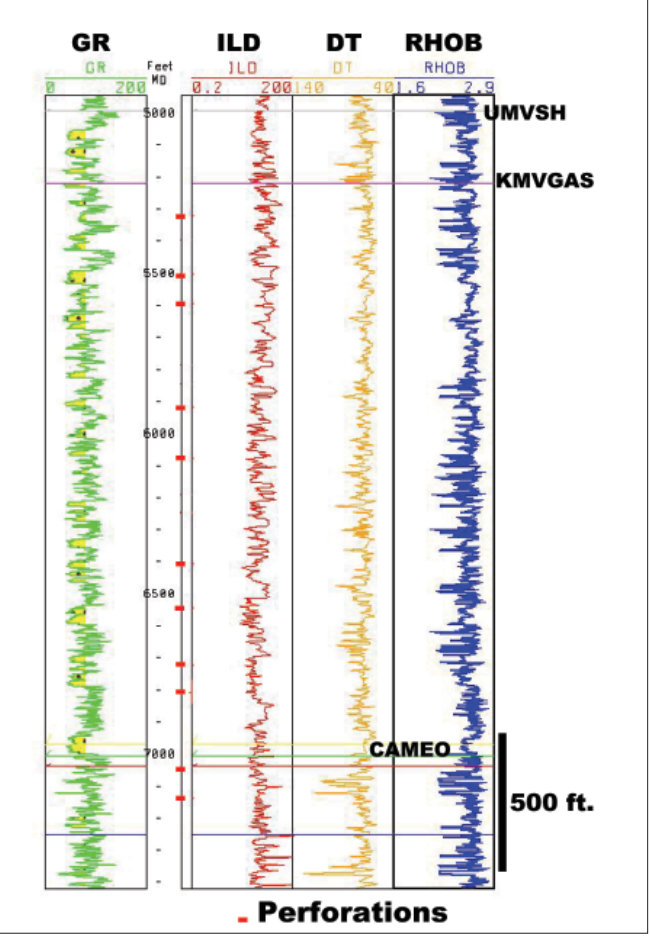


Figure 1. Log type at the Mesaverde reservoir interval. UMVSH=Upper Mesaverde shale, a regional marker. KMVGAS=top of gas production. CAMEO=top of Cameo, the lower gas-producing interval which contains coal beds. GR=Gama ray, ILD=induction. DT=sonic. RHOB=density. Short red dashes=perforations.

as the static window for the P-wave seismic data. For the pure S-wave data, a 200-ms window around the Upper Mesaverde shale was chosen as the static window. For the converted Swave data, a static window of 1200-1400 ms was chosen. The corrections are designed in the static window and then applied to the entire seismic volume.

We applied three corrections to the P-wave and converted S-wave data in the following order: a correlation time shift, a shaping filter, and a comparison gain. The corrections to the pure S-wave data were a correlation time shift and a compari-

The correlation time shift is a static time shift that aligns base and monitor surveys in time; the shaping filter makes the wavelet of each data set the same, and the comparison gain corrects for amplitude-scaling differences between the base and monitor surveys.

Spectral decomposition attributes

As a basic definition, spectral decomposition refers to any method that produces a continuous time-frequency analysis from a seismic trace. Thus, it is possible to have a frequency spectrum in every time sample from a seismic trace.

There are a variety of spectral decomposition methods. We used a method based on matching-pursuit decomposition which finds a bestmatched wavelet from a wavelet dictionary to represent each component of a signal and which enhances the spectral resolution without side-lobe effects. Spectral decomposition provides abundant data to analyze. We performed the time-lapse interpretation using two well-known spectraldecomposition attributes, the peak frequency and the peak amplitude. The peak frequency corresponds to the frequency value at which the maximum amplitude occurs, and this maximum amplitude is the peak amplitude. Figure 3 shows the concept of these attributes at two particular time samples of a seismic trace.

From a static point of view, a low peak frequency corresponds to thicker sandstone intervals and a high peak frequency corresponds to thinner sandstone intervals. This is in agreement with the work of Chung and Lawton (1995) who observed that the peak frequency slightly increases as the layer thickness decreases.

After extrapolating the above considerations about peak frequency from the static point of view (change in thickness) to the time-lapse point of view (where velocity changes cause changes in apparent temporal thickness), we conclude that these attributes are suitable for time-lapse interpretation because they summarize the information content of the full frequency spectrum.

Noise evaluation

We perform time-lapse seismic interpretation with spectral decomposition by obtaining average time-lapse maps of the differences of the peak-frequency

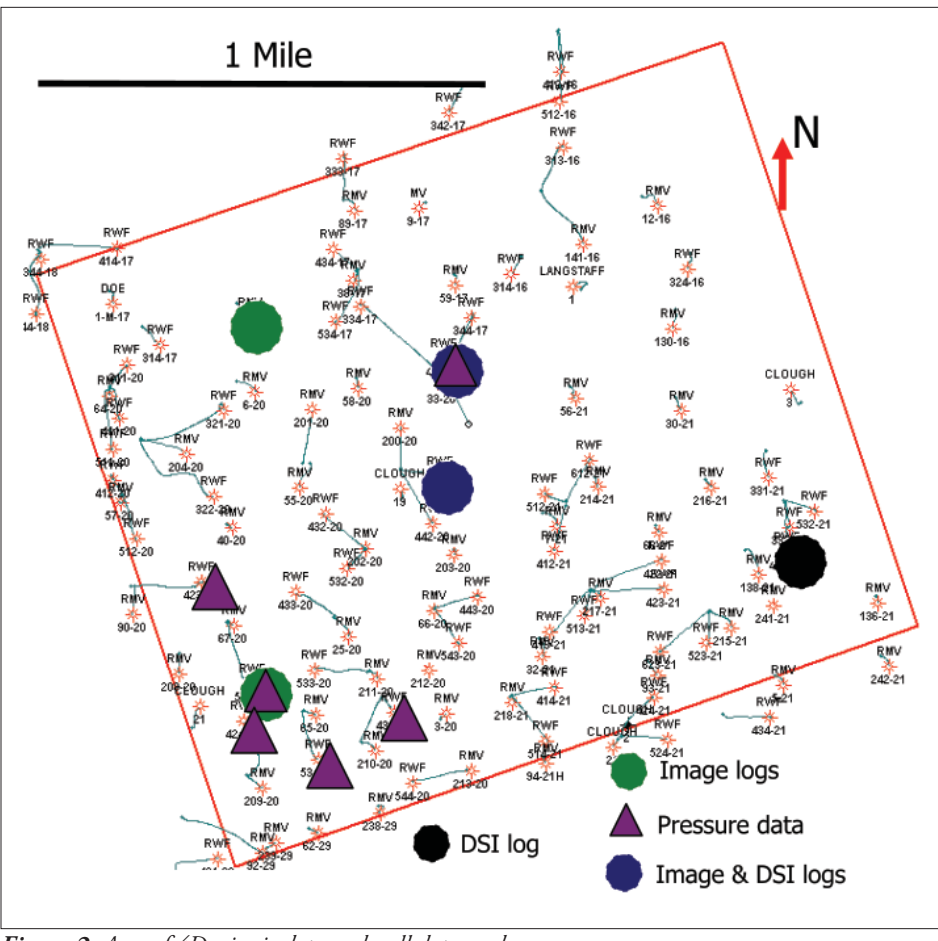


Figure 2. Area of 4D seismic data and well data used.

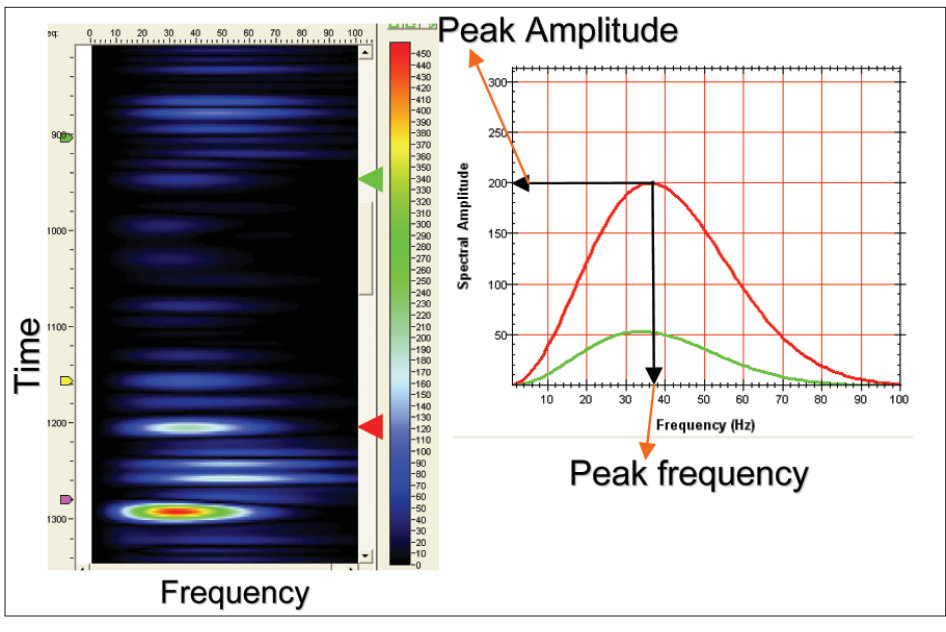


Figure 3. Spectral decomposition of a seismic trace (left). The color bar indicates the spectral amplitude. The amplitude spectrum of two time samples illustrates the concept of peak frequency and peak amplitude (right).

and peak-amplitude spectral attributes.

The average time-lapse maps of the differences in both attributes were calculated using the following formula, which

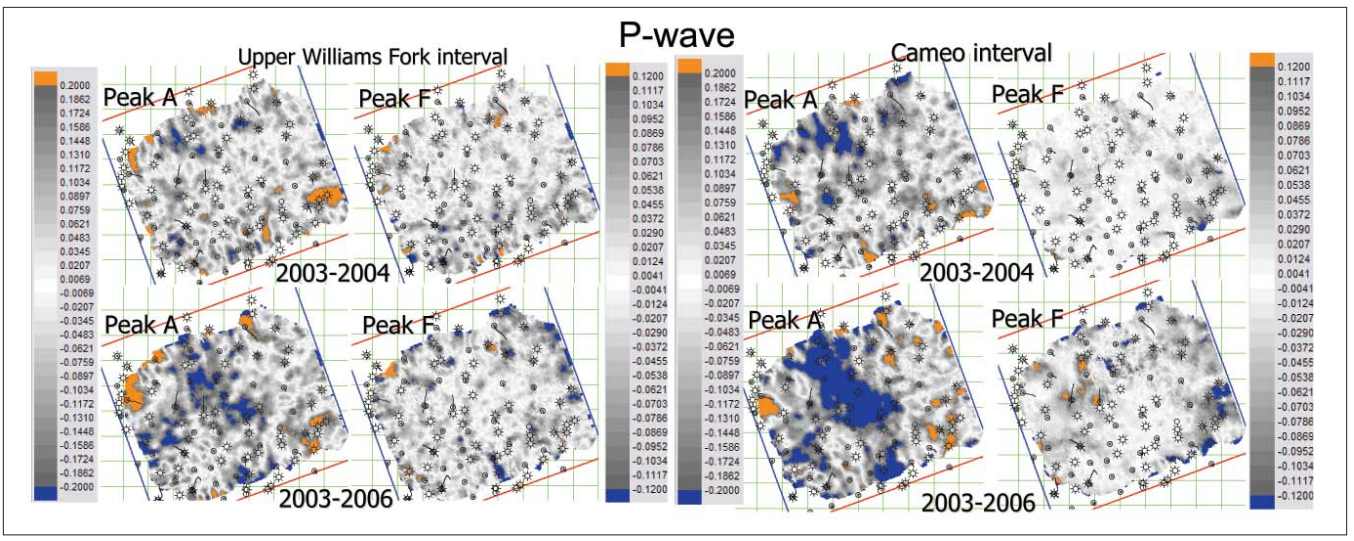


Figure 4. Average peak amplitude (peak A) and peak frequency (peak F) time-lapse maps, 2003–2004 and 2003–2006 from Upper Williams Fork interval (left panel) and the Cameo interval (right panel) with P-wave seismic data. The color bar highlights the values just beyond the noise cutoff previously determined. Note the big negative peak-amplitude anomaly from time-lapse 2003–2006 in the Cameo interval at the central part of the area.

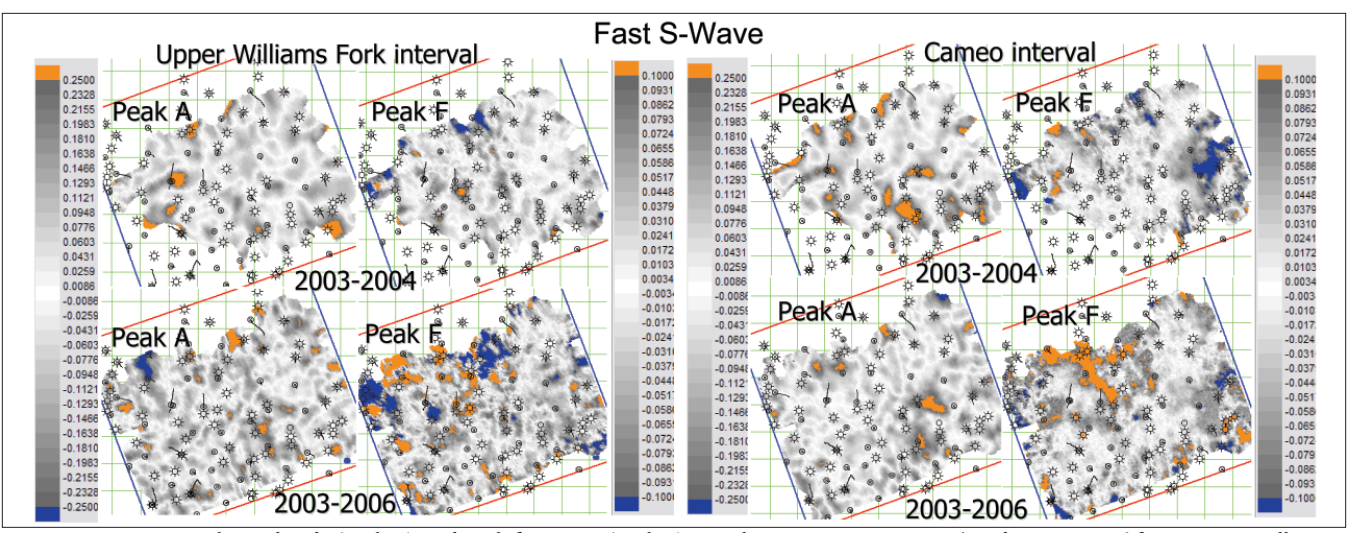


Figure 5. Average peak amplitude (peak A) and peak frequency (peak F) time-lapse maps, 2003–2004 and 2003–2006 from Upper Williams Fork interval (left panel) and the Cameo interval (right panel) with fast, pure S-wave seismic data. The color bar highlights the values just beyond the noise cutoff previously determined.

gives the fractional differences by subtraction of the average spectral attributes between the time-lapse surveys.

Time-lapse maps of the differences of (peak A or F) = peak (A or F) [(2006 or 2004) - 2003]/peak (A or F) (2003), where peak (A or F) refers to the estimate of the average peak amplitude (A) or the peak frequency (F) time-lapse map and 2006 or 2004 refers to the time-lapse 2006-2003 or 2004-2003 maps, respectively.

Before performing the time-lapse interpretation with the spectral-decomposition attributes at the reservoir interval, we need to determine the amount of these differences that corresponds to background noise. To estimate the background noise, we first obtained average time-lapse maps of the differences of the spectral attributes in a window above the reservoir and from these time-lapse maps we estimated a level of noise or background noise cutoff value until no anomaly is

observed in the entire area of the map. We assume that this background noise is the same in the reservoir interval; only anomalies or differences beyond this background noise cutoff will be considered for analysis and interpretation of the time-lapse maps obtained at the reservoir interval.

We estimate a noise cutoff value above the reservoir for both peak-amplitude and peak-frequency attributes for each seismic data set.

Time-lapse maps from the reservoir interval

We analyzed the time-lapse pairs of seismic surveys 2003–2004 and 2003–2006, using P-wave and pure S-wave data and the pair 2003–2006 using converted S-wave data. In both types of S-waves, the fast and slow modes were analyzed separately.

For better time-lapse comparison, we grouped the res-

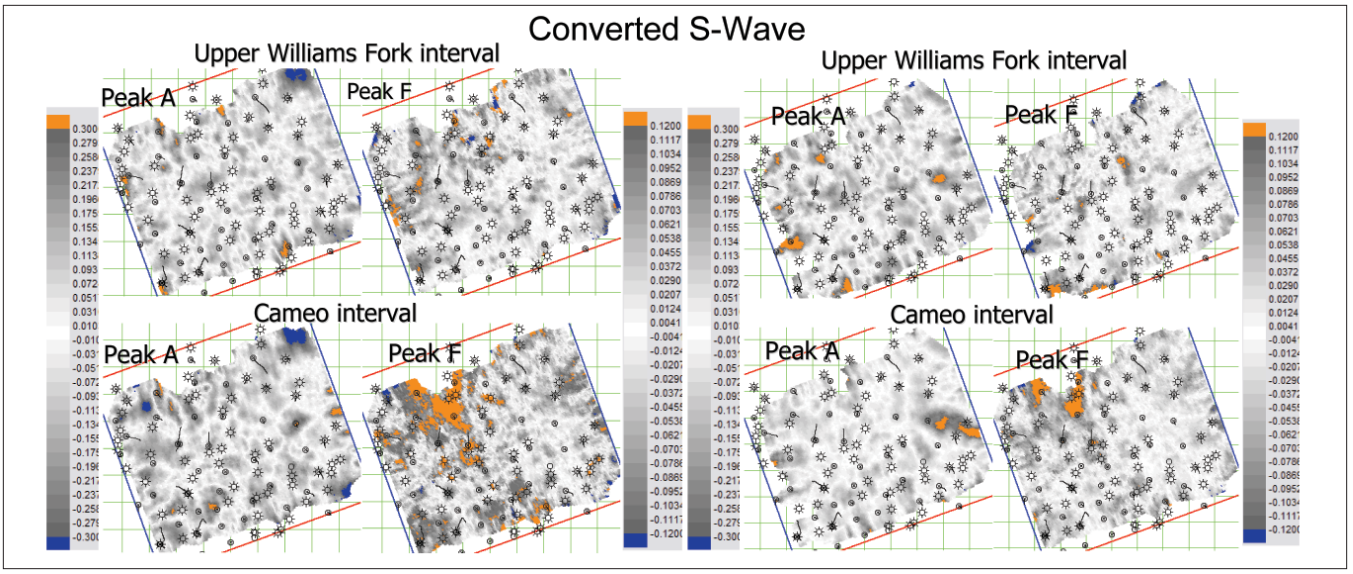


Figure 6. Average peak amplitude (peak A) and peak frequency (peak F) time-lapse maps, 2003–2006 from Upper Williams Fork interval and the Cameo interval with fast, converted S-wave seismic data (left panel) and slow, converted S-wave seismic data (right panel). The color bar highlights the values just beyond the noise cutoff previously determined.

ervoir into two intervals, the Upper Williams Fork interval from the top of the gas production to the top of the Cameo interval, and the Cameo interval itself (from top of Cameo to base of Cameo). Although gas production comes commingled from these two intervals, they represent different reservoir settings. The Upper Williams Fork interval was deposited in a meandering fluvial system and the Cameo interval in a lower coastal plain. Therefore, separately comparing these intervals helps to enhance the time-lapse differences. We obtained average time-lapse maps of the differences of peak frequency and peak amplitude from these two intervals.

We found that the time-lapse 2003–2006 shows the biggest differences in both spectral attributes. Figures 4–6 show the most relevant time-lapse maps obtained in both reservoir intervals. We point out that in these maps the color bar highlights the values just beyond the background noise cutoff values determined previously.

The time-lapse maps revealed that the stronger anomalies with both attributes are in the Cameo interval. Using P-wave data, we found a negative peak-amplitude anomaly in the central part of the study area (right of Figure 4). Using both converted and pure S-wave data, we found a similar positive peak-frequency anomaly in the Cameo interval (Figures 5 and 6).

Time-lapse maps and gas production

Gas production is one of the few parameters to compare with the time-lapse maps in this particular case. After obtaining the time-lapse maps using peak-amplitude and peak-frequency attributes, we compared them with an accumulated gas production map and an estimated ultimate reserves (EUR) map by well. This comparison showed a good correlation between the best wells in terms of EUR and the large negative peak-amplitude anomaly that occurs at the Cameo interval time-lapse 2003–2006 with P-wave data. On the other hand,

positive anomalies in peak-frequency maps from the Cameo interval using converted and pure fast shear-wave data are related to the wells with the highest accumulated gas production in the time-lapse 2003–2006. No anomaly is observed in areas where small amounts of gas were produced. Figure 7 shows these relationships. In the following section, we discuss possible explanations and interpret these observed relationships.

Discussion of results

We have observed that peak-amplitude anomalies are related to P-wave data and peak-frequency anomalies are related to S-wave data and, in both cases, the stronger anomalies occur in the Cameo interval. Additionally, good correlation exists between the highest EUR wells and the amplitude anomaly and between the best producing wells during the time lapse analyzed and the frequency anomaly. Consequently, we conclude that the Cameo interval is most sensitive to time-lapse changes. This is due to the presence of coals in this interval, which are more sensitive to stress than the surrounding sand-stone and shale lithologies.

P-waves are affected by compressibility and rigidity; meanwhile S-waves are affected by rigidity. P-waves are sensitive to the presence of fluids, in this case gas, which affects the bulk compressibility. Shear waves are unaffected by gas but instead are more affected by changes in stress that in this case could be related to fractures. Therefore, we interpret that the positive anomalies in peak frequency could be related to fractured areas where the fractures were open during initial gas production but progressively, due to pressure drawdown, became closed making the rock stiffer. This increased the S-wave velocity and, consequently, also the peak frequency. This behavior agrees with the concept that the anisotropy is frequency-dependent; thus, for any given fracture size, the anisotropy decreases as frequency increases (Maultzsch et al., 2003).

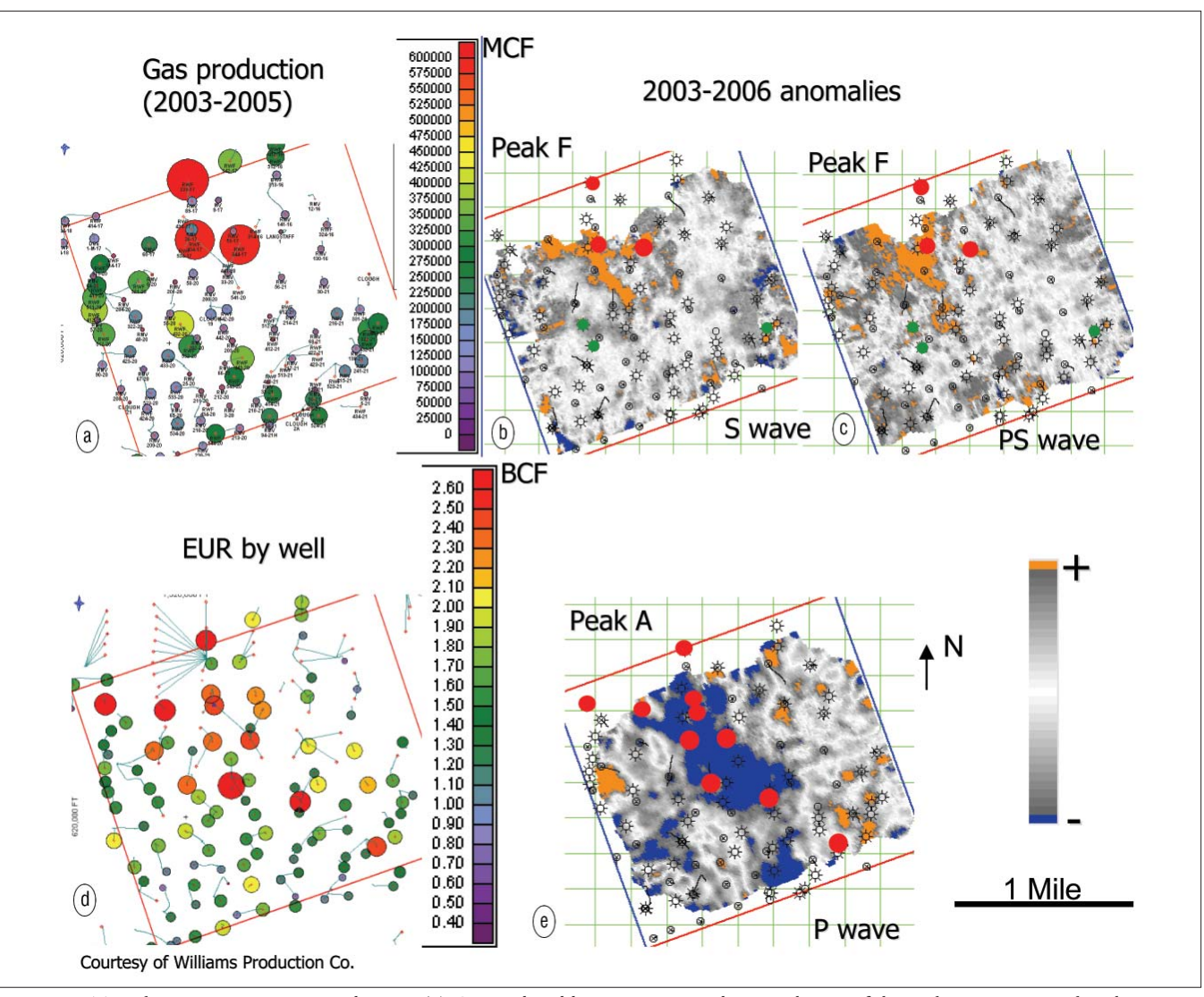


Figure 7. Time-lapse maps versus gas production. (a) Gas produced between 2003 and 2005; the size of the circles is proportional to the gas produced per thousand cubic feet of gas (MCF). (b) and (c) Peak-frequency time-lapse maps 2003–2006 with pure S-wave data and converted S-wave data, respectively. The red dots correspond to the highest production wells in (a) and the green dots to the second-ranked production wells. (d) Estimated ultimate reserves (EUR) by well; the size of the circles is proportional to the estimated reserves in billion cubic feet of gas (BCF). (e) Peak-amplitude time-lapse map 2003–2006 with P-wave data; red dots correspond to the best EUR wells in (d). Note the good relation between the best producing wells and the anomalies of the time-lapse peak-frequency maps and between the best EUR wells and the anomalies in the time-lapse peak-amplitude map.

With reference to the amplitude anomaly detected with P-wave data, according to previous forward modeling, a positive time-lapse anomaly must have occurred. Instead, a negative anomaly is observed. However, surprising is the fact that this negative anomaly correlates with the best EUR wells. To explain this behavior, it must be remembered that P-waves are sensitive to gas content and that just a small amount of gas significantly affects the compressibility of the rock. Additionally, this anomaly must be interpreted with other information. Using image logs, Matesic (2006) found that faults have a strike of approximately N35°W and that the open natural and induced fractures occur at approximately N75°W. Comparing these directions with the structural map to the top of the Cameo interval, we found that the main alignment shown in the map correlates with the fault direction found by Matesic. Therefore, this alignment may correspond to a

fault with throw less than seismic resolution. Consequently, due to the fractured nature of this reservoir, natural fractures should occur related to this fault. Notice that this is precisely the orientation of the amplitude anomaly and the best EUR wells are located there. For these reasons, we interpret that the large amplitude anomaly is related to an area with a principal fault with many associated natural fractures. Natural fractures increased the productivity of the wells in this area, where not all the gas has been totally expelled and small amounts are still left in the fractures, causing a "gas effect" in the P-wave data. A factor that helps to create this gas effect is the presence of coals, which we presume are desorbing gas and creating a "gas recharge" in the fault area. This explains why this anomaly is negative and areally more extended than the peak frequency anomaly.

In conclusion, time-lapse, peak-frequency anomalies are

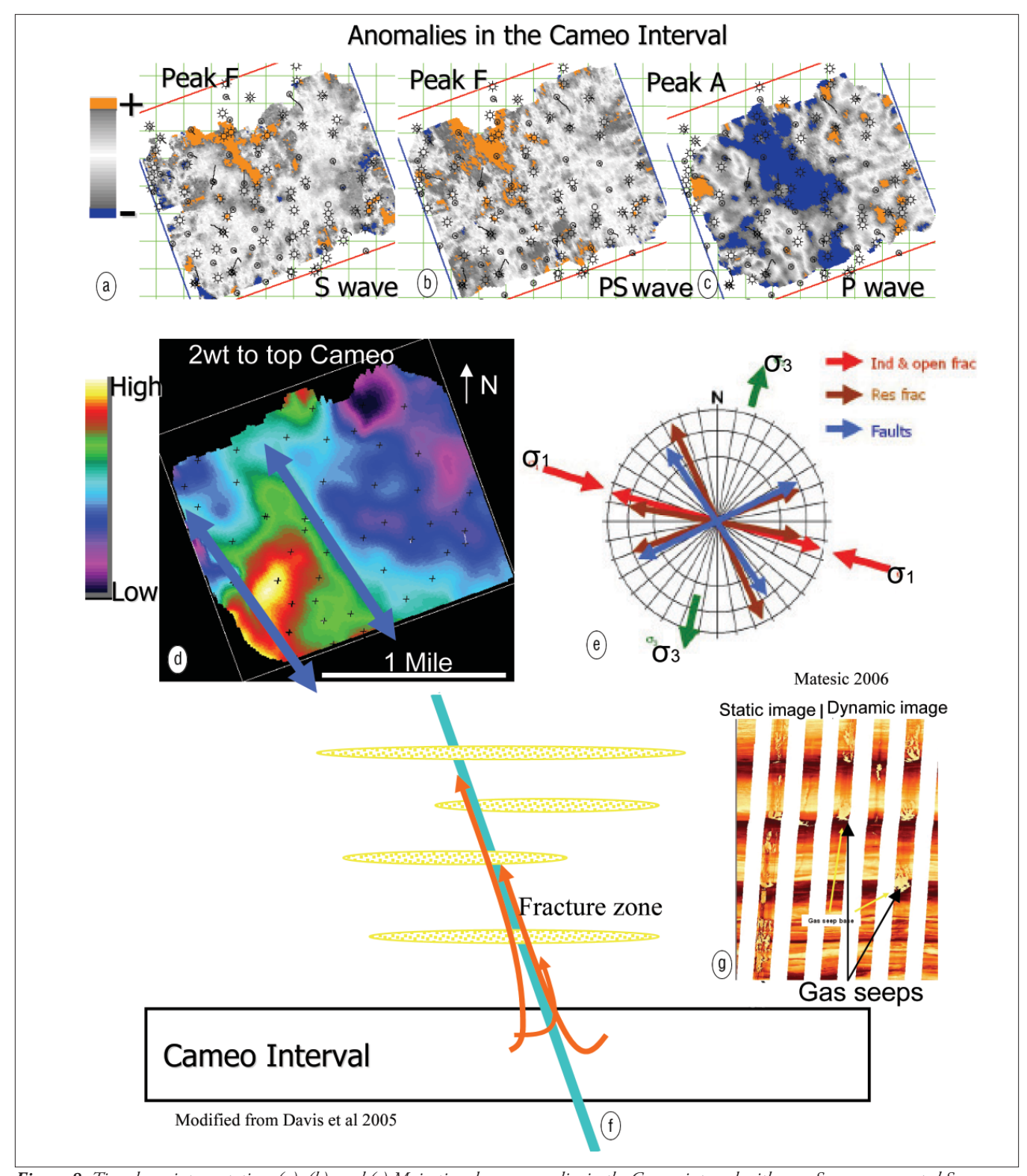


Figure 8. Time-lapse interpretation. (a), (b), and (c) Main time-lapse anomalies in the Cameo interval with pure S-wave, converted S-wave, and P-wave seismic data, respectively. (d) Structural map in two-way time (2wt) to the top of the Cameo interval; warm colors mean high areas and cool colors are low areas. (e) Directions of structural features interpreted by Matesic (2006). (f) Schematic showing the Cameo interval interpreted as an active source of gas that migrates upward to the upper reservoirs through faults and fractures. (g) Gas seeps observed in image logs, which prove the actual gas migration.

related to the highest changes in rock stiffness as a consequence of fractures closing during gas production; meanwhile, the time-lapse peak amplitude anomalies are related to

a gas recharge as a consequence of gas desorbed from coals in the area of the principal fault and fractures related to it.

Observations of our analysis reinforce the theory that the

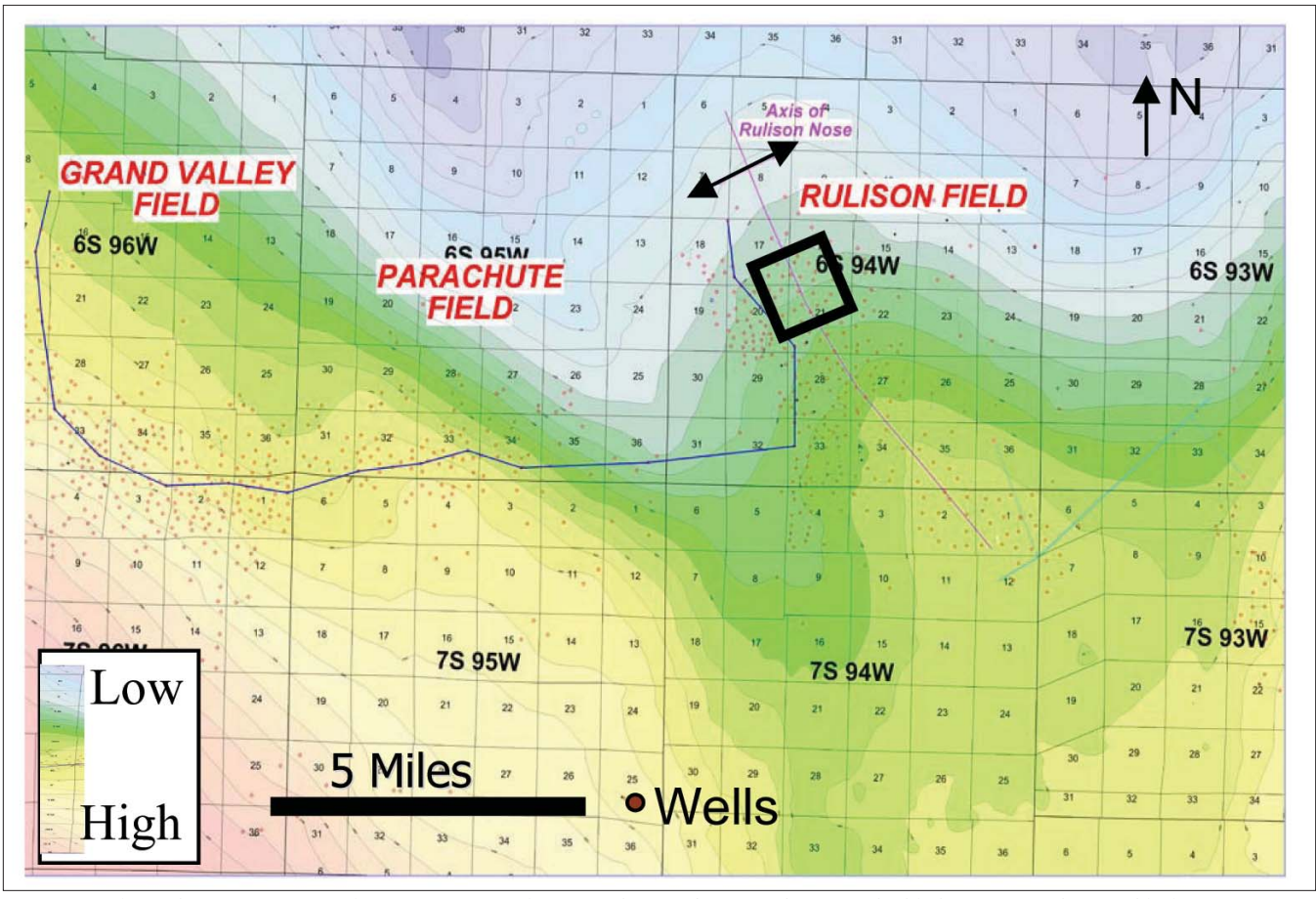


Figure 9. The study area in a regional context. Structural map on the top of Mesaverde Group, highlighting our study area (black square) at Rulison Field. Note how the trend of the main fold axis in the whole area correlates with the NW-SE trend of the time-lapse anomaly maps found in this study. In this direction or along similar trends, we proposed the development of the field outside of our study area. (Modified from Cumella and Ostby)

faults and their related fractures play an important role in the gas production at Rulison Field. Additionally, and taking the idea of Davis et al. (2005), the Cameo interval is interpreted as an active source of gas that migrates upward to the upper reservoirs. Evidence of this upward migration is shown by gas seeps observed in image logs. Figure 8 synthesizes the interpretation concepts described here.

Considering the results shown and the fact that our study area is a small part of Rulison Field, we suggest that future development must be concentrated in this trend or similar trends that can be found in surrounding areas. This concept of looking into areas with this type of alignment or trend also can be applied to similar fields in this area or to other basins. Figure 9 shows our study area in an extended regional context with the suggested prospective trend to develop.

Suggested reading. Geology of the Basin-Centered Gas Accumulation, Piceance Basin, Colorado by Cumella and Ostby (Rocky Mountain Association of Geologists, 2003). "Seismic time-fre-

quency spectral decomposition by matching pursuit" by Yanghua (Geophysics, 2007). "Modeling frequency-dependent seismic anisotropy in fluid-saturated rock with aligned fractures: implication of fracture size estimation from anisotropic measurements" by Maultzsch et. al (*Geophysical Prospecting*, 2003). "Spectral decomposition of 4D seismic data" by Zhao and Johnston (SEG 2006 *Expanded Abstracts*). "Structural and stratigraphic controls on Mesaverde reservoir performance: Rulison Field, Garfield County, Colorado" by Matesic, (Master's thesis, Colorado School of Mines, 2007). "Time-lapse seismic study for tight-gas sands, Rulison Field, Colorado" by Davis et al., (*Nafta*, 2005). "Amplitude responses of thin beds: Sinusoidal approximation versus Ricker approximation" by Chung and Lawton (Geophysics, 1995). **TLE**

Acknowledgments: We thank the sponsors of the Reservoir Characterization Project of Colorado School of Mines.

Corresponding author: Nelson.Rojas@ecopetrol.com.co